Instantaneous global plate motion model from 12 years of continuous GPS observations

Linette Prawirodirdjo and Yehuda Bock

Cecil H. and Ida M. Green Institute of Geophysics and Planetary Physics, Scripps Institution of Oceanography, La Jolla, California, USA

Received 16 December 2003; revised 12 May 2004; accepted 10 June 2004; published 11 August 2004.

[1] We estimate a global plate motion model for 17 major and minor tectonic plates solely on the basis of analysis of data from 106 globally distributed continuous GPS stations, spanning the period from January 1991 to July 2003. Site positions estimated from 24-hour segments of data are aligned day-by-day to the International GPS Service (IGS) realization of the ITRF2000 reference frame using a similarity transformation, thereby ensuring that the ITRF2000 no-net-rotation condition is preserved. Linear velocities of a carefully selected set of stations are estimated from the position time series, along with annual and semiannual fluctuations and position offsets due to GPS instrument changes. A white noise plus flicker noise model is applied to estimate realistic uncertainties for the site velocities, which are then propagated into the derived plate motion model parameters. We also examine the vertical velocities in the site selection process. At the Scripps Orbit and Permanent Array Center we have implemented a procedure whereby the plate motion model is updated on a regular (monthly) basis to improve its precision and reliability as new data become available and as a baseline against which anomalous motions can be detected. *INDEX TERMS:* 1206 Geodesy and Gravity: Crustal movements—interplate (8155); 1243 Geodesy and Gravity: Space geodetic surveys; 3040 Marine Geology and Geophysics: Plate tectonics (8150, 8155, 8157, 8158); 1247 Geodesy and Gravity: Terrestrial reference systems; *KEYWORDS:* continuous GPS, global plate motions

Citation: Prawirodirdjo, L., and Y. Bock (2004), Instantaneous global plate motion model from 12 years of continuous GPS observations, *J. Geophys. Res.*, *109*, B08405, doi:10.1029/2003JB002944.

1. Introduction

[2] The concept of rigid tectonic plates in relative (horizontal) motion over an underlying asthenosphere [*McKenzie and Parker*, 1967; *Morgan*, 1968; *Le Pichon et al.*, 1973] is the current paradigm and fundamental underpinning of geological, geophysical, and geodynamic studies. Early plate motion models defined relative angular velocities for the major plates [*Chase*, 1972, 1978; *Minster et al.*, 1974] from mid-ocean ridge spreading rates (inferred from magnetic lineations), transform fault azimuths, and earthquake slip vectors. These early models imposed a geometric condition that the lithosphere have no net rotation relative to the underlying asthenosphere [*Solomon and Sleep*, 1974] or a physical condition based on the fixed hot spot hypothesis [*Wilson*, 1963, 1965; *Morgan*, 1971, 1972; *Minster and Jordan*, 1978]. The NUVEL-1A model [*DeMets et al.*, 1994], with the associated No-Net-Rotation NUVEL-1A (NNR-NUVEL-1A) plate motion model [*Argus and Gordon*, 1991], is the current definitive geologic plate model. Since geologic plate models incorporate data from the Pliocene to Recent time, they provide representative values over the last 3 Myr.

0148-0227/04/2003JB002944$09.00

[3] Space geodesy developed within a decade of modern plate tectonic theory and provided, initially from satellite laser ranging (SLR) [*Christodoulidis et al.*, 1985] and very long baseline interferometry (VLBI) [*Herring et al.*, 1986], directly observed "snapshot" instantaneous measurements of the motion of the tectonic plates from repeated estimates of site positions. In the 1980s the international geodetic community began to define terrestrial reference frames that were realized by positions and velocities of a global network of stations estimated from a combination of space geodetic methods. Underlying these frames were external velocity constraints derived from geologic plate motion models (e.g., NUVEL-1A). The International Terrestrial Reference Frame (ITRF) series of terrestrial reference frames, developed under the umbrella of the International Earth Rotation Service (IERS), used geologic rates as constraints from ITRF88 to ITRF97 [*Altamimi et al.*, 2002]. However, the proliferation of global geodetic stations provided by the Global Positioning System (GPS) and the accuracy of space geodetic positioning have evolved to the point where discrepancies began to appear between geodetic velocities and velocities predicted by the geologic models (e.g., NUVEL-1A) [e.g., *Larson et al.*, 1997; *DeMets and Dixon*, 1999; *Wdowinski et al.*, 2001].

[4] *Sella et al.* [2002] presented the REVEL plate motion model based solely on a carefully selected set of space geodetic data (primarily GPS) and avoiding zones of plate

boundary and diffuse deformation. Their model was referenced to ITRF97, constrained to the underlying NUVEL-1A geologic model. ITRF2000, the most recent and next in the series after ITRF97, is the first one to be free of any plate tectonic model, although it maintains the no-net-rotation condition by aligning the orientation time evolution of the ITRF2000 to that of NNR-NUVEL-1A [*Altamimi et al.*, 2003]. This decouples the long-term (~3 Myr) geologic from the short-term (~20 years) geodetic rates, providing improved opportunity to compare the two. Other advantages of ITRF2000 over ITRF97 are the use of a larger and better distributed network of stations, a longer time series, and fewer inconsistent local ties. One ''absolute'' plate kinematic model with respect to ITRF2000 is APKIM2000.0 maintained by H. Drewes at the Deutsches Geodatisches Forschunginstitut (DGFI), which describes the Euler vectors for 12 plates (http://dgfi2.dgfi.badw-muenchen.de/geodis/GDYN/apkim.html).

[5] Plate tectonic theory is an idealization and does not describe broad zones of plate boundary deformation. Recent work has attempted to develop more refined models of deformation that combine the motions of rigid plates and deforming zones. *Drewes* [1998] combined space geodetic velocity fields and plate boundary deformation in California, Japan, the Mediterranean, and South America to construct an absolute plate motion model. *Kreemer and Holt* [2001] and *Kreemer et al.* [2003] used primarily GPS observations and observed strain rates inferred from Quaternary fault slip rates in Asia to construct a NNR surface motion model. Plate tectonics also assumes perfectly horizontal motions of rigid plates, although vast areas are subject to vertical motions from tectonic processes (e.g., mountain building) and nontectonic processes such as postglacial rebound [e.g., *Peltier*, 1995]. Space geodesy is now providing vertical deformation rates with a sufficient level of precision [e.g., *Nikolaidis*, 2002] to further refine plate tectonic theory and provide the essential underpinnings for geodynamic studies.

[6] The use of GPS data is now widespread in the study of plate tectonics and crustal deformation, with continuous GPS (CGPS) instruments deployed at hundreds of global stations and thousands of regional stations around the world. Global CGPS activities are coordinated by the International GPS Service (IGS) (http://igscb.jpl.nasa.gov). IGS realizes ITRF2000 by adopting the ITRF2000 coordinates and velocities of 53 globally distributed core stations (the set of core sites has recently been revised to include 99 stations) at the epoch 1998.0, with respect to which the IGS analysis centers compare and compute daily site positions, orbital and Earth orientation parameters, and other products. The IGS network and products provide the unifying framework for regional CGPS networks that monitor surface deformation related to, for example, the seismic cycle at plate boundaries. CGPS was first used to measure coseismic displacements following the M_w 7.3 Landers, California, earthquake in 1992 with data from the Southern California Permanent GPS Geodetic Array (PGGA) [*Bock et al.*, 1993; *Blewitt et al.*, 1993]. Further analysis of CGPS and field GPS surveys led to the observation of transient postseismic motion throughout the region in the following months [*Shen et al.*, 1994]. Coseismic and long-period postseismic deformations are now routinely observed by the Southern California Integrated GPS Network (SCIGN) [e.g., *Nikolaidis*, 2002] and other CGPS networks spanning plate boundaries, for example, the Japanese Geographical Survey Institute nationwide GPS Earth Observation Network (GEONET) array [*Miyazaki et al.*, 1998]. In the last few years, CGPS has also detected aseismic slow earthquakes [*Dragert et al.*, 2001; *Melbourne et al.*, 2002; *Miller et al.*, 2002], precursory transient slip not detected by traditional seismic methods [*Melbourne and Webb*, 2002], small changes in present-day relative plate motions [*Norabuena et al.*, 1999], and seismic motions [*Nikolaidis et al.*, 2001; *Larson et al.*, 2003; *Bock et al.*, 2004].

[7] For our study we use CGPS data and metadata from 1991 to 2003 archived and analyzed daily at the Scripps Orbit and Permanent Array Center (SOPAC) to calculate a global plate motion model with respect to the IGS realization of ITRF2000 (IGS2000) [*Altamimi et al.*, 2002]. Our ITRF2000 velocity field is shown in Figure 1. Our goal is to provide a CGPS-based model of current global plate motion which is easily used/replicated by other researchers because it is based on a data set which is readily available to the public, spans a long period of time, and is kept up to date (current data are collected and processed daily). We follow an approach similar to *Sella et al.*'s [2002] development of the REVEL plate motion model, based solely on a carefully selected set of space geodetic data (primarily GPS) and avoiding zones of plate boundary and diffuse deformation. We also examine vertical velocities in the site selection process to ensure long-term site stability and to identify anomalous site motions. The differences between our study and *Sella et al.*'s [2002] are as follows:

[8] 1. Our analysis relies solely on CGPS data and metadata archived and analyzed at SOPAC and includes 3.5 more years of data and several new sites (*Sella et al.* [2002] used data collected through 2000).

[9] 2. Our analysis is referenced to ITRF2000, a significant improvement in precision compared to ITRF97 used by *Sella et al.* [2002]. Our site positions are estimated from 24 hours of GPS phase and pseudorange data and are aligned day-by-day to the IGS realization of the ITRF2000 reference frame using a seven-parameter similarity transformation.

[10] 3. Our time series analysis of daily site positions includes the modeling of annual and semiannual effects (this was not done by *Sella et al.* [2002]) as described by *Nikolaidis* [2002], thereby improving the precision of estimated site velocities. The inclusion of seasonal effects also improves the detection of position outliers, the selection of sites for use in estimating the plate motion parameters, and the quantification of the white noise plus flicker noise model (the same noise model applied by *Sella et al.* [2002]) for the estimated daily site positions.

[11] 4. We use the GAMIT/GLOBK software suite to estimate a self-contained (in-house) set of site positions, satellite orbits, Earth orientation, and integer-cycle phase ambiguities using the ''double-differencing'' approach. *Sella et al.* [2002] used the GIPSY OASIS II, release 5.0 software developed at the Jet Propulsion Laboratory (JPL), relying on the nonfiducial satellite orbits and clock files provided by JPL and then applying the ''point-positioning'' approach using these external products. Thus our GPS analysis provides a completely independent deter-

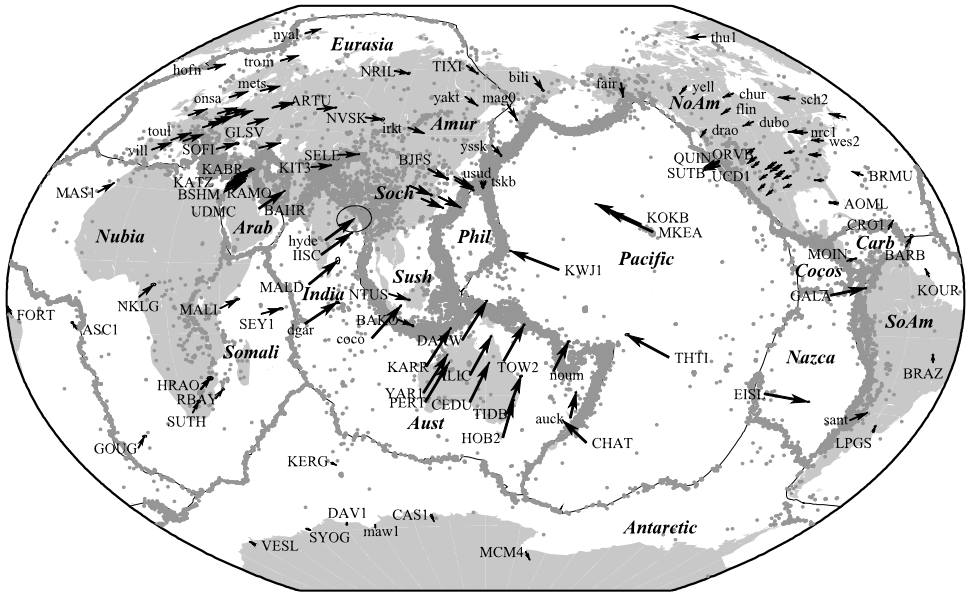

Figure 1. Positions and ITRF2000 velocities, with 95% confidence error ellipses, of stations used in this study, using a white noise plus flicker noise model for the underlying position time series. Stations labeled in capital letters were used to estimate the plate angular velocities listed in Table 2. Gray dots indicate ($M_w \geq 4$) earthquakes from1973 to 2000 from National Earthquake Information Center (http://wwwneic.cr.usgs.gov/) and delineate plate boundary locations. For clarity, some site labels have been omitted.

mination of the daily positions of many of the same sites used by *Sella et al.* [2002].

[12] The velocity field underlying our plate motion model is continuously being refined and updated as the position time series grow with time and increase in number as new CGPS sites are established and/or made publicly available. Our goal is not so much to provide a static list of Euler vectors but more to document the (growing) set of CGPS stations which can be considered to be located on rigid tectonic plates (as opposed to deforming plate boundary zones) and from them provide a basis, in the form of robust velocity estimates based on long-lived, continually updated CGPS station time series, for an evolving definition of rigid plate motions. Our time series analysis allows us to quickly identify core stations that experience anomalous motions and to quantify these motions. Station fair (Fairbanks, Alaska), is an example of a core IGS station that is well known to have experienced coseismic offsets and postseismic deformation due to the 2002 Denali fault earthquake (Figure 2). Our velocity field can be considered as an external check on the IGS realization of ITRF2000 (SOPAC's velocity field was not used in the development of ITRF2000) that can rapidly identify problematic sites and suggest new sites that may be suitable in strengthening the realization of ITRF2000.

2. Data Analysis

[13] We reanalyzed the SOPAC-archived data in a consistent and uniform manner as described by *Nikolaidis* [2002] for the period 1991–2001 and continued the identical analysis procedure at SOPAC until the present time (circa July 2003). The reanalysis was preceded by an extensive reconciliation of the metadata in the SOPAC relational database management system during which a significant number of blunders were detected and repaired, reducing the number of estimated offsets in the position time series, thereby improving the precision of estimated site velocities. While the data comprise several networks established and maintained by various institutions, they are processed at SOPAC in a consistent manner and are tied together by a uniform reference frame, ITRF2000, as realized by the IGS. In this paper we present and discuss the velocities of 140 stations (Figure 1 and Table 1) which are relevant to our global plate motion model. Out of these 140 stations, 106 are used to estimate rigid plate motions. With a few exceptions the stations discussed here have time series that are 4 years or more in length, and most have time series that are at least 6 years long. The longest time series spans 12 years.

[14] The GPS data are analyzed in 24-hour segments using the GAMIT software version 10.06 [*King and Bock*, 2002] as described in detail by *Nikolaidis* [2002], resulting in daily site positions, as well as satellite orbits, Earth orientation parameters, troposphere parameters, and integer-cycle phase ambiguities. The sites are distributed in 20 subnetworks, including 4 global subnetworks and 16 regional subnetworks, with a number of overlapping sites in each subnetwork [*Zhang*, 1996]. All solutions for each day are then combined using the GLORG module of the GLOBK version 5.06 software [*Herring*, 2000], and the reference frame is applied to the solution by performing a seven-parameter transformation to align it to ITRF2000, defined as a set of stations whose positions as a function of time are specified by IGS (via initial positions and linear velocities). The resulting daily position estimates in ITRF2000 are plotted as a time series for each station (http://sopac.ucsd.edu/cgi-bin/refinedJavaTimeSeries.cgi), which is updated every week with current data. From the daily position time series

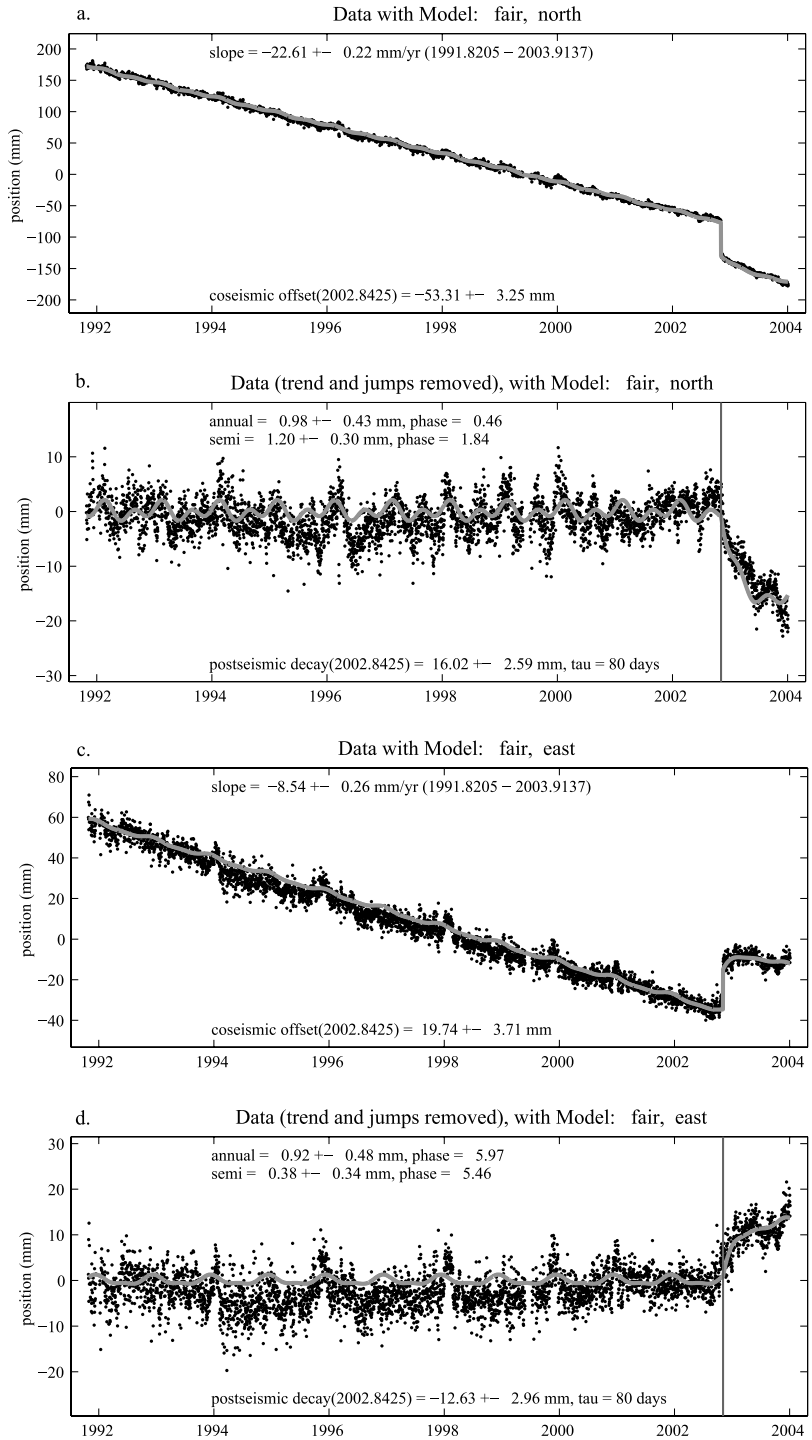

Figure 2. Example time series showing the (a and b) north and (c and d) east position time series for station fair (Fairbanks, Alaska) with modeled (gray lines) trends and annual and semiannual fluctuations. Figures 2b and 2d show data with the trend and coseismic jumps removed.

we estimate the stations' linear velocities, taking into account offsets and seasonal fluctuations as described by *Nikolaidis* [2002]. Seasonal fluctuations of the station positions are modeled by fitting an annual term to stations that have at least 2 years of data and also a semiannual term for stations that have at least 1 year of data. Modeling the seasonal terms allows more accurate estimation of the stations' linear velocities [*Blewitt and Lavallee*, 2002]. This is especially important for stations that have a relatively short time series and/or large seasonal fluctuations. For stations which experience postseismic relaxation, an exponentially decaying term is estimated for the horizontal velocity components (for example, Figure 2). In some cases where a station experiences coseismic and postseismic deformation, changes in the linear velocity are also estimated. Stations which exhibit coseismic and postseismic motion are gener-

Table 1. Station Coordinates, Observed ITRF2000 Velocities, 1σ Uncertainties, and Residuals[a]

Site	Δt,[b] years	Longitude, °E	Latitude, °N	ITRF2000 Velocity, mm/yr			Residual,[c] mm/yr	
				East	North	Vertical	E	N
				Amuria (Amur)				
BJFS	3.6	115.893	39.609	29.9 ± 0.7	−14.1 ± 0.7	−2.2 ± 1.5	1.1	−0.4
DAEJ	4.4	127.375	36.399	27.5 ± 0.7	−14.8 ± 0.6	−0.5 ± 1.3	−0.4	0.0
SUWN	5.7	127.054	37.276	27.5 ± 0.6	−14.6 ± 0.4	−1.8 ± 1.0	−0.2	0.3
tskb[d]	9.6	140.088	36.106	−3.3 ± 0.4	−10.2 ± 0.4	−1.3 ± 0.6	−29.3	5.2
usud	10.8	138.362	36.133	1.4 ± 0.5	−9.3 ± 0.4	0.7 ± 0.9	−24.9	6.1
yssk	4.0	142.717	47.030	13.5 ± 0.6	−15.0 ± 0.6	−1.3 ± 1.4	−8.2	0.5
				Antarctica (Anta)				
CAS1[d]	9.1	110.520	−66.283	2.0 ± 0.3	−9.9 ± 0.3	4.6 ± 0.9	0.5	0.2
DAV1[d]	9.1	77.973	−68.577	−1.9 ± 0.3	−5.1 ± 0.3	3.2 ± 0.6	0.5	0.2
KERG[d]	8.7	70.256	−49.352	5.9 ± 0.4	−3.8 ± 0.3	4.8 ± 0.8	0.7	0.5
MCM4[d]	8.5	166.669	−77.838	8.7 ± 0.3	−11.6 ± 0.3	2.2 ± 1.1	−0.3	−0.5
SYOG	4.2	39.584	−69.007	−3.7 ± 0.9	2.5 ± 0.7	3.5 ± 1.7	−0.5	−0.6
VESL	5.0	−2.842	−71.674	−0.1 ± 0.7	8.6 ± 0.7	−1.5 ± 1.2	−0.6	−1.6
maw1	5.6	62.871	−67.605	−1.8 ± 0.6	−3.3 ± 0.5	1.4 ± 1.1	1.0	−1.5
				Arabia (Arab)				
BAHR[d]	7.1	50.608	26.209	30.7 ± 0.3	27.9 ± 0.3	−1.6 ± 0.8	−0.4	0.2
DRAG	2.9	35.392	31.593	23.6 ± 0.9	17.8 ± 0.4	−0.5 ± 2.3	0.1	−2.2
ELAT	6.0	34.921	29.509	25.1 ± 0.5	19.6 ± 0.4	−0.8 ± 0.7	−0.1	−0.1
ELRO	3.3	35.771	33.182	23.1 ± 0.7	20.3 ± 0.5	−0.4 ± 1.6	1.0	0.1
GILB	5.0	35.417	33.479	22.4 ± 0.6	19.3 ± 0.4	−0.8 ± 1.2	0.6	−0.7
KATZ	6.0	35.688	32.995	22.5 ± 0.6	21.2 ± 0.4	−1.7 ± 0.8	0.2	1.1
UDMC	1.2	36.285	33.510	21.7 ± 1.6	21.5 ± 0.9	0.4 ± 3.4	−0.2	1.0
				Australia (Aust)				
ALIC	5.6	133.886	−23.670	31.8 ± 0.5	56.4 ± 0.4	3.7 ± 1.2	−0.4	−0.5
CEDU[d]	5.5	133.810	−31.867	28.9 ± 0.4	56.7 ± 0.4	4.6 ± 0.1	−0.0	−0.2
DARW	11.1	131.133	−12.844	36.6 ± 0.6	57.2 ± 0.3	−1.9 ± 0.7	0.5	−0.0
HOB2[d]	9.1	147.439	−42.805	13.7 ± 0.6	54.6 ± 0.5	2.1 ± 0.7	−0.9	0.6
KARR	5.6	117.097	−20.981	38.3 ± 0.5	55.3 ± 0.6	3.0 ± 1.7	−0.8	−1.0
PERT[d]	10.0	115.885	−31.802	38.8 ± 0.3	56.7 ± 0.3	−0.1 ± 0.7	0.5	0.6
TIDB[d]	11.2	148.980	−35.399	18.0 ± 0.8	54.4 ± 0.6	1.3 ± 0.8	−0.8	1.1
TOW2	5.6	147.056	−19.269	29.0 ± 0.7	52.9 ± 0.5	1.1 ± 1.2	−0.5	−1.2
YAR1[d]	10.4	115.347	−29.047	39.3 ± 0.4	55.7 ± 0.3	1.0 ± 0.8	0.3	−0.3
auck[d]	7.9	174.834	−36.603	3.3 ± 0.6	37.9 ± 0.3	1.0 ± 0.8	−2.0	−1.0
coco	7.1	96.834	−12.188	44.9 ± 0.6	47.2 ± 0.6	1.6 ± 0.9	1.7	−2.1
noum	5.6	166.410	−22.270	19.6 ± 1.0	43.2 ± 0.5	0.6 ± 1.6	−1.8	−1.4
				Caribbean (Carb)				
BARB	3.2	−59.609	13.088	12.0 ± 1.1	15.5 ± 1.0	0.8 ± 1.5	−1.2	0.5
CRO1	9.6	−64.584	17.757	10.8 ± 0.4	12.8 ± 0.3	−0.4 ± 0.9	0.4	0.0
MOIN	2.1	−83.094	9.987	13.3 ± 0.8	3.4 ± 0.4	−4.7 ± 1.4	−0.8	−0.4
mana	3.1	−86.2490	12.149	6.5 ± 1.3	8.9 ± 0.9	4.9 ± 1.7	−6.3	6.7
				Eurasia (Eura)				
ARTU	4.0	58.560	56.430	25.3 ± 0.7	4.8 ± 0.5	−2.3 ± 2.1	−0.3	−1.0
BOR1	8.9	17.074	52.277	20.6 ± 0.2	14.0 ± 0.1	−1.3 ± 0.6	0.1	−0.0
GLSV	5.5	30.497	50.364	22.5 ± 0.4	12.1 ± 0.3	−1.3 ± 1.1	−0.8	0.2
GOPE	7.9	14.786	49.914	20.6 ± 0.3	14.6 ± 0.2	0.9 ± 1.0	0.0	0.3
GRAS	8.1	6.921	43.755	20.5 ± 0.2	14.6 ± 0.2	0.2 ± 0.4	−0.1	−0.4
JOZE	10.0	21.032	52.097	21.3 ± 0.2	13.7 ± 0.2	−1.3 ± 0.6	0.1	0.2
KIT3[d]	8.9	66.885	39.135	28.0 ± 0.4	3.9 ± 0.3	−3.3 ± 0.7	−0.4	0.3
MDVO	7.3	37.224	56.028	23.4 ± 0.4	10.2 ± 0.3	0.0 ± 1.2	0.3	−0.5
NRIL	2.8	88.360	69.362	22.6 ± 0.7	−3.2 ± 0.9	−0.4 ± 3.0	−0.5	−1.0
NVSK	2.4	83.235	54.841	26.5 ± 1.0	−2.2 ± 1.1	6.3 ± 3.6	−0.3	−1.3
OBER	4.6	11.280	48.086	20.5 ± 0.3	15.0 ± 0.3	−0.4 ± 1.0	0.1	0.3
POTS[d]	8.8	13.066	52.379	19.7 ± 0.2	14.3 ± 0.1	−0.2 ± 0.6	0.1	−0.2
SELE	5.9	77.017	43.179	28.3 ± 0.5	2.0 ± 0.4	−3.0 ± 1.0	−0.1	1.2
SOFI	1.7	23.395	42.556	24.3 ± 1.3	11.7 ± 0.9	7.0 ± 3.8	0.6	−1.5
TIXI	4.8	128.866	71.635	17.1 ± 0.6	−11.6 ± 0.7	−5.2 ± 1.7	−0.3	0.2
WTZR[d]	7.6	12.879	49.144	20.5 ± 0.2	14.6 ± 0.2	−0.7 ± 0.6	0.1	0.1
ZECK	5.9	41.565	43.788	26.5 ± 0.3	10.2 ± 0.2	2.2 ± 0.9	0.5	0.5
ZWEN[d]	7.9	36.759	55.699	23.3 ± 0.3	10.5 ± 0.3	−2.4 ± 0.8	0.2	−0.3
hers	11.9	0.336	50.867	16.6 ± 0.4	15.6 ± 0.4	−3.8 ± 1.1	−0.8	0.1
hofn	5.9	−15.198	64.267	12.5 ± 0.4	15.7 ± 0.4	8.5 ± 1.1	3.3	0.1
irkt[d]	7.9	104.316	52.219	24.6 ± 0.4	−8.0 ± 0.3	0.0 ± 0.8	−1.5	−1.6
mag0	5.7	150.770	59.576	11.9 ± 0.6	−22.4 ± 0.6	−3.1 ± 1.0	−4.8	−7.6
mets	11.1	24.395	60.218	20.3 ± 0.2	12.2 ± 0.2	4.0 ± 0.6	0.6	−0.8
nyal[d]	12.5	11.865	78.930	11.2 ± 0.2	14.1 ± 0.2	6.3 ± 0.5	0.8	−0.5

Table 1. (continued)

Site	Δt,[b] years	Longitude, °E	Latitude, °N	ITRF2000 Velocity, mm/yr			Residual,[c] mm/yr	
				East	North	Vertical	E	N
onsa[d]	12.2	11.926	57.395	17.2 ± 0.1	14.3 ± 0.1	1.1 ± 0.5	−0.8	−0.3
toul	3.9	1.481	43.561	19.4 ± 0.5	15.7 ± 0.3	−1.5 ± 1.2	−0.3	0.3
trom[d]	12.5	18.938	69.663	15.3 ± 0.2	14.4 ± 0.3	1.1 ± 0.5	−0.2	0.6
vill[d]	8.6	−3.952	40.444	19.3 ± 0.3	15.6 ± 0.2	−1.6 ± 0.7	−0.1	−0.0
			India					
IISC	7.8	77.570	13.021	41.8 ± 0.5	32.7 ± 0.4	−0.6 ± 1.0	−0.2	−0.2
MALD	3.3	73.526	4.189	41.1 ± 1.2	34.8 ± 2.0	12.0 ± 5.0	1.3	0.7
hyde	0.5	78.551	17.417	38.6 ± 10.3	32.9 ± 8.0	28.8 ± 19.2	−4.1	−0.4
dgar[d]	7.2	72.370	−7.270	48.5 ± 1.0	31.2 ± 0.6	1.7 ± 1.2	12.0	−3.2
			Nazca (Nazc)					
EISL	9.3	−109.383	−27.148	67.1 ± 0.7	−8.4 ± 0.4	−2.0 ± 1.1	−1.0	−1.1
GALA	6.8	−90.304	0.743	51.2 ± 0.7	10.5 ± 0.4	1.8 ± 1.2	0.9	1.1
			North America (Noam)					
AMC2	4.8	−104.525	38.803	−12.7 ± 0.7	−7.4 ± 0.5	3.3 ± 1.3	1.5	0.1
AOML	5.7	−80.162	25.735	−11.2 ± 0.7	2.3 ± 0.4	0.3 ± 1.2	−0.3	0.5
BRMU[d]	10.4	−64.696	32.370	−11.8 ± 0.4	7.8 ± 0.2	−0.5 ± 0.7	0.5	0.2
DQUA	6.3	−94.290	34.111	−13.5 ± 0.3	−3.3 ± 0.3	1.5 ± 1.1	−0.0	0.4
GODE[d]	10.2	−76.827	39.022	−14.6 ± 0.2	2.9 ± 0.2	−0.9 ± 0.5	0.3	−0.2
HBRK	8.3	−97.294	38.305	−13.8 ± 0.3	−5.1 ± 0.2	0.9 ± 0.7	0.7	−0.2
HKLO	8.3	−95.863	35.683	−14.2 ± 0.3	−4.3 ± 0.2	2.4 ± 0.7	−0.3	0.1
HVLK	7.2	−99.107	37.652	−14.7 ± 0.3	−6.0 ± 0.2	0.4 ± 0.8	−0.5	−0.5
LMNO	8.4	−97.481	36.685	−13.7 ± 0.3	−4.4 ± 0.2	0.6 ± 0.7	0.3	0.5
MDO1[d]	10.2	−104.015	30.681	−12.1 ± 0.2	−7.5 ± 0.2	1.2 ± 0.5	−0.2	−0.1
NDSK	4.0	−95.638	37.381	−14.4 ± 0.4	−4.5 ± 0.3	−1.5 ± 1.4	−0.1	−0.3
PATT	6.2	−95.719	31.778	−12.9 ± 0.4	−4.0 ± 0.3	0.2 ± 0.9	−0.2	0.2
PLTC	8.4	−104.726	40.182	−14.9 ± 0.2	−7.7 ± 0.2	1.7 ± 0.6	−0.4	−0.1
PRCO	7.7	−97.519	34.980	−13.2 ± 0.3	−5.5 ± 0.3	−0.5 ± 1.0	0.3	−0.5
SAV1	4.7	−81.696	32.139	−12.3 ± 0.6	1.5 ± 0.5	0.3 ± 1.1	0.7	0.4
STJO	11.2	−52.678	47.595	−15.5 ± 0.3	11.9 ± 0.2	0.4 ± 0.5	−0.7	0.1
TCUN	5.7	−103.609	35.085	−13.4 ± 0.4	−6.7 ± 0.3	2.1 ± 1.0	−0.2	0.5
TMGO	8.7	−105.233	40.131	−14.9 ± 0.3	−8.2 ± 0.2	2.5 ± 0.9	−0.4	−0.4
USNO	6.3	−77.066	38.919	−15.1 ± 0.4	3.1 ± 0.3	0.6 ± 0.9	−0.2	0.1
WHN1	4.8	−103.329	42.739	−14.4 ± 0.4	−6.8 ± 0.3	4.2 ± 1.2	0.9	0.3
WLCI	4.8	−87.052	40.808	−14.2 ± 0.7	−1.5 ± 0.4	3.9 ± 1.7	1.3	−0.5
WSMN	6.3	−106.350	32.407	−12.3 ± 0.3	−7.6 ± 0.2	0.7 ± 0.8	−0.1	0.6
algo[d]	12.5	−78.071	45.956	−16.6 ± 0.5	1.3 ± 0.4	5.0 ± 0.6	0.2	−1.3
bili	3.9	166.438	68.076	9.4 ± 0.7	−21.1 ± 0.7	0.3 ± 1.6	3.3	−0.1
chur	8.1	−94.089	58.759	−18.3 ± 0.4	−4.8 ± 0.3	9.3 ± 0.8	1.1	−1.1
drao[d]	12.4	−119.625	49.323	−13.6 ± 0.2	−11.4 ± 0.2	2.1 ± 0.6	1.1	1.3
dubo	6.8	−95.866	50.259	−18.2 ± 0.4	−5.4 ± 0.3	3.7 ± 1.4	−0.5	−1.1
fair[d]	11.8	−147.499	64.978	−8.6 ± 0.3	−22.6 ± 0.2	0.8 ± 0.8	1.2	−2.8
flin	7.2	−101.978	54.726	−17.8 ± 0.3	−8.3 ± 0.2	3.5 ± 1.0	0.3	−1.7
nrc1	8.1	−75.624	45.454	−16.4 ± 0.3	2.4 ± 0.2	3.0 ± 0.7	0.2	−1.1
sch2	5.9	−66.833	54.832	−17.8 ± 0.6	7.3 ± 0.4	12.9 ± 1.1	0.3	0.5
thu1[d]	7.6	−68.788	76.537	−22.9 ± 0.3	3.9 ± 0.3	1.6 ± 1.1	−1.8	−2.2
wes2[d]	10.5	−71.493	42.613	−14.7 ± 0.3	3.3 ± 0.3	−0.8 ± 0.6	1.0	−1.8
yell[d]	12.5	−114.481	62.481	−17.6 ± 0.2	−12.6 ± 0.2	4.4 ± 0.6	0.1	−1.6
			Nubia (Nubi)					
GOUG	5.0	−9.881	−40.349	19.8 ± 1.2	18.0 ± 0.6	−10.4 ± 1.8	−0.6	1.2
HARB	2.7	27.707	−25.887	17.7 ± 1.7	15.8 ± 1.1	0.7 ± 2.2	0.4	−0.8
HARK	3.1	27.708	−25.887	18.8 ± 1.5	16.1 ± 1.0	−1.9 ± 2.4	1.4	−0.4
HRAO[d]	6.9	27.687	−25.890	18.4 ± 0.7	15.8 ± 0.4	0.0 ± 0.9	1.1	−0.8
MAS1[d]	9.2	−15.633	27.764	16.1 ± 0.5	16.4 ± 0.3	1.8 ± 1.1	−0.4	0.2
NKLG	3.3	9.672	0.354	21.4 ± 1.5	18.1 ± 0.7	−1.5 ± 2.1	−0.9	0.5
SUTH	5.3	20.811	−32.380	15.8 ± 0.9	17.4 ± 0.7	2.8 ± 1.3	−0.8	0.3
			Pacific (Pacf)					
CHAT[d]	7.8	−176.566	−43.956	−41.4 ± 0.4	32.0 ± 0.3	1.2 ± 0.8	0.2	0.6
KOKB[d]	12.8	−159.665	22.126	−61.3 ± 0.5	32.1 ± 0.3	1.9 ± 1.1	0.6	−0.8
KWJ1[d]	6.4	167.730	8.722	−69.7 ± 0.7	27.7 ± 0.4	−3.5 ± 1.2	−1.0	−0.0
MKEA	5.9	−155.456	19.801	−62.7 ± 0.7	32.4 ± 0.4	−2.4 ± 1.1	−0.6	−0.4
THTI	5.2	−149.609	−17.577	−65.3 ± 1.2	31.8 ± 0.7	0.3 ± 2.0	0.2	−0.6
farb	9.4	−123.001	37.697	−39.2 ± 0.3	24.1 ± 0.2	0.0 ± 0.9	1.6	−2.2
			Sierra (Sier)					
ORVB	6.7	−121.500	39.555	−22.2 ± 0.3	−5.9 ± 0.2	−0.2 ± 0.4	−0.1	−0.4
SUTB	6.4	−121.821	39.206	−22.8 ± 0.4	−5.3 ± 0.3	−0.9 ± 0.4	−0.3	−0.0
UCD1	6.5	−121.751	38.536	−23.0 ± 0.4	−4.7 ± 0.3	−4.8 ± 0.4	0.3	0.6

Table 1. (continued)

Site	Δt,[b] years	Longitude, °E	Latitude, °N	ITRF2000 Velocity, mm/yr East	ITRF2000 Velocity, mm/yr North	ITRF2000 Velocity, mm/yr Vertical	Residual,[c] mm/yr E	Residual,[c] mm/yr N
				Sinai (Sina)				
BSHM	4.8	35.023	32.779	21.8 ± 0.6	18.6 ± 0.4	0.5 ± 1.5	−0.2	0.0
JSLM	1.7	35.203	31.771	22.5 ± 0.5	20.1 ± 0.4	9.8 ± 1.0	−0.5	1.3
KABR	5.1	35.145	33.023	21.7 ± 0.5	18.8 ± 0.3	−3.2 ± 1.2	0.1	0.0
LHAV	2.4	34.866	31.378	22.9 ± 0.9	17.5 ± 0.6	3.2 ± 1.6	−0.6	−1.0
RAMO	5.2	34.763	30.598	23.9 ± 0.4	17.7 ± 0.3	1.9 ± 0.9	−0.4	−0.7
TELA	6.0	34.781	32.068	23.4 ± 0.4	18.5 ± 0.3	−2.6 ± 0.9	0.7	0.0
				Somali (Soma)				
MALI[d]	7.8	40.194	−2.996	26.4 ± 1.2	13.4 ± 0.5	1.5 ± 1.6	−0.9	0.9
RBAY	2.8	32.078	−28.796	15.9 ± 0.8	14.2 ± 0.8	5.3 ± 1.6	−0.7	−0.9
SEY1	7.7	55.479	−4.674	29.1 ± 1.5	7.7 ± 0.6	−0.6 ± 2.2	2.7	0.6
				South America (Soam)				
ASC1[d]	7.2	−14.412	−7.951	−5.4 ± 0.9	9.7 ± 0.6	−1.2 ± 1.2	−0.4	0.2
BRAZ	8.2	−47.878	−15.948	−3.6 ± 0.6	11.5 ± 0.5	−1.0 ± 1.0	0.5	0.3
FORT[d]	10.2	−38.426	−3.877	−4.8 ± 0.6	11.2 ± 0.3	0.3 ± 1.2	−0.4	0.1
KOUR[d]	10.7	−52.806	5.252	−4.1 ± 0.5	11.5 ± 0.3	3.4 ± 1.6	0.3	0.4
LPGS	8.1	−57.932	−34.907	−2.1 ± 0.6	10.6 ± 0.5	0.0 ± 0.0	0.1	−0.3
sant[d]	11.2	−70.669	−33.150	18.5 ± 0.5	15.3 ± 0.5	3.8 ± 1.5	19.5	5.2
				South China (Soch)				
SHAO[c]	7.8	121.200	31.100	32.5 ± 0.4	−15.1 ± 0.3	−1.2 ± 0.8	0.4	−0.2
WUHN	7.5	114.357	30.532	32.5 ± 0.5	−13.1 ± 0.4	−2.9 ± 1.1	−0.5	0.5
XIAN	5.1	109.222	34.369	32.9 ± 0.6	−13.0 ± 0.5	−4.0 ± 1.3	−0.2	−0.4
				Sunda Shelf (Sush)				
BAKO	5.4	106.849	−6.491	21.9 ± 0.8	−9.1 ± 0.7	5.9 ± 2.3	−1.2	4.4
NTUS	5.9	103.680	1.346	29.4 ± 0.8	−8.8 ± 0.6	−0.5 ± 1.1	0.8	2.5

[a]Stations are grouped by region. Site codes in capital letters were used to calculate rotation parameters for the respective plates/blocks denoted in bold letters.
[b]Length of time series as of July 2003.
[c]Residual velocities are relative to the respective plates/blocks.
[d]IGS core stations used in realization of ITRF2000.

ally not used in Euler vector calculations. Station Fairbanks (fair) in Alaska (Figure 2), for example, is one of the "core" IGS stations, which are used by IGS to define the ITRF2000 frame, but is clearly not located on a rigid plate. All parameters are estimated with full white noise plus flicker noise covariances based on a maximum likelihood estimation (MLE) noise analysis of the GPS position time series [*Williams*, 2003; *Williams et al.*, 2004]. Their uncertainties can thus be considered realistic estimates based on analysis of the noise at individual stations. The a priori coordinates for the daily GAMIT analysis are based on the current station positions as predicted by our modeling of the time series, taking into account all the parameters described in this paragraph (http://sopac.ucsd.edu/processing/coordinates/).

[15] The Euler vectors for 17 tectonic plates are estimated by minimizing their velocities relative to the ITRF2000. Selection of stations for each plate was done by trial and error, with our initial choices being guided by other published studies of global plate motions [e.g., *Beavan et al.*, 2002; *Sella et al.*, 2002]. We avoid stations located near plate boundaries or those known to have exhibited coseismic or postseismic motions. Past studies [e.g., *Dixon et al.*, 1996] suggest that a good fit to a rigid plate Euler vector is indicated by residual station velocities roughly equal to the GPS velocity uncertainties. This holds true in our study, with most of the velocity residuals being well below 1 mm/yr and as low 0.1 mm/yr for the best constrained stations. We thus adopt a rule of thumb of including in the rigid plate motion estimates only stations whose velocity residuals are less than the 2σ velocity uncertainties. We have made a few exceptions to this rule for plates with a sparse distribution of stations. By applying this criterion to the station selection process, we obtain χ^2_ν (χ^2 per degree of freedom) values of $\sim$1.0 for the well-determined stations. The stations we used, with their ITRF2000 velocities and residuals relative to their respective plates, are listed in Table 1, our estimated Euler vectors relative to ITRF2000 are listed in Table 2, and relative angular velocities for adjacent plate pairs are listed in Table 3. Every 4 weeks we reestimate the ITRF2000 Euler vectors listed in Table 2. This evolving list of Euler vectors can be viewed online at (http://sopac.ucsd.edu/cgi-bin/poleRotationValues.cgi). We expect that with time, the precision of these estimates will improve, particularly for the currently less well determined plates, because of the lengthening of the time series and also the availability of new CGPS stations.

3. Discussion

[16] The ITRF2000 site velocity uncertainties from our analysis (using the white noise plus flicker noise model) are much lower than the corresponding uncertainties in the ITRF2000 values published by the IERS and used by the IGS (Figures 3 and 4) (and are also significantly lower than

Table 2. Plate Angular Velocities Relative to ITRF2000[a]

Plate	Longitude, °E	Latitude, °N	ω deg/Myr	Error Ellipse, deg			χ^2_ν	N
				σ_{maj}	σ_{min}	Azimuth		
Amur	−126.646	63.899	0.316 ± 0.021	10.85	0.88	146	0.7	3
Anta	−125.655	60.683	0.222 ± 0.006	0.77	0.56	8	1.6	6
Arab	3.576	51.341	0.546 ± 0.014	1.49	0.28	157	1.4	7
Aust	37.590	33.472	0.618 ± 0.003	0.93	0.18	154	1.2	9
Carb	−90.741	33.648	0.314 ± 0.021	2.80	0.81	146	1.0	3
Eura	−99.691	57.246	0.260 ± 0.002	0.81	0.18	52	1.1	18
Indi	−41.986	45.720	0.487 ± 0.015	12.11	0.73	29	0.7	2
Nazc	−101.161	45.410	0.652 ± 0.010	1.83	0.57	93	8.8	2
Noam	−84.702	−3.583	0.200 ± 0.003	0.87	0.25	101	1.3	22
Nubi	−82.685	51.627	0.790 ± 0.004	1.82	0.92	175	0.8	7
Pacf	110.161	−63.832	0.670 ± 0.003	0.59	0.28	2	1.2	5
Sier	50.854	−56.539	0.673 ± 0.284	11.17	0.22	71	1.5	3
Sina	10.887	49.230	0.627 ± 0.128	7.72	0.23	145	1.7	6
Soam	−135.798	−21.086	0.108 ± 0.003	6.33	1.80	171	0.4	5
Soch	−117.403	61.428	1.088 ± 0.008	8.13	0.63	135	1.1	3
Soma	−106.378	51.305	0.326 ± 0.017	3.87	1.40	36	1.6	3
Sush	−86.799	32.565	0.462 ± 0.064	7.00	0.84	113	4.0	2

[a]Plate abbreviations are given in Table 1; ω is positive for counterclockwise (CCW) rotation; σ_{maj} and σ_{min} are the 1σ lengths in degrees of the major and minor axes of the pole error ellipse, with the azimuth of the major axis given CCW from east; χ^2_ν values are the sum of squared weighted-residuals, normalized by the degrees of freedom; and N is the number of stations used to estimate block rotation parameters. All uncertainties are unscaled.

the velocity uncertainties reported by *Sella et al.* [2002]). This is partly due to the longer time interval spanned by our analysis but can also be explained by our relying on a single measurement type (CGPS), carefully screened, and analyzed in a uniform manner. The ITRF2000 is based on a heterogeneous set of space geodetic data, derived by combining, in a weighted manner, the independent solutions provided by several analysis centers. This is one of the strengths and major accomplishments of ITRF2000 but also one of its weaknesses. These types of combinations are influenced by seemingly mundane factors such as local site ties between monuments observed by different space geodetic techniques and inaccurate metadata. Furthermore, ITRF2000 does not yet take into account seasonal variations and may include

Table 3. Relative Angular Velocities for Adjacent Plate Pairs

Plate Pair[a]	Longitude, °E	Latitude, °N	ω, deg/Myr	Error Ellipse, deg		
				σ_{maj}	σ_{min}	Azimuth
Amur-Eura	−25.253	45.433	0.093 ± 0.023	43.0	4.4	171
Anta-Aust	40.486	−13.352	0.638 ± 0.009	0.77	0.18	156
Anta-Nazc	86.144	−36.464	0.446 ± 0.016	0.61	0.27	90
Anta-Nubi	−39.502	−3.481	0.109 ± 0.010	3.82	1.09	74
Anta-Pacf	−84.002	65.176	0.875 ± 0.009	0.16	0.15	41
Anta-Soam	−63.833	85.049	0.233 ± 0.009	0.72	0.55	64
Arab-Eura	23.198	27.507	0.439 ± 0.019	0.96	0.35	13
Arab-Soma	27.243	20.135	0.459 ± 0.034	0.78	0.33	42
Aust-Eura	46.355	11.111	0.639 ± 0.005	0.94	0.17	149
Aust-Pacf	4.176	61.488	1.072 ± 0.006	0.41	0.11	12
Aust-Soma	47.592	7.105	0.696 ± 0.020	0.85	0.16	149
Aust-Soch	43.335	4.641	0.663 ± 0.011	0.91	0.17	150
Carb-Noam	70.680	70.508	0.198 ± 0.024	8.16	1.28	140
Carb-Nazc	65.537	−54.495	0.350 ± 0.031	3.89	0.72	29
Carb-Soam	−70.144	46.353	0.294 ± 0.024	3.35	0.86	94
Eura-Noam	−54.411	72.343	0.242 ± 0.005	0.32	0.14	173
Eura-Nubi	−22.099	20.098	0.051 ± 0.006	5.05	0.95	114
Eura-Pacf	−79.448	62.645	0.922 ± 0.005	0.20	0.05	36
Indi-Eura	−17.652	24.222	0.318 ± 0.017	16.97	1.09	9
Indi-Aust	73.937	0.764	0.564 ± 0.018	3.44	0.62	100
Indi-Soma	−5.802	16.725	0.325 ± 0.032	15.32	1.03	6
Noam-Nubi	87.592	−78.932	0.217 ± 0.007	1.02	0.23	93
Noam-Pacf	−75.826	50.163	0.766 ± 0.006	0.13	0.06	36
Noam-Soam	−54.793	9.514	0.160 ± 0.006	1.12	0.31	135
Nubi-Soam	−43.250	62.037	0.271 ± 0.007	1.63	0.88	140
Nubi-Soma	26.371	−32.156	0.102 ± 0.021	4.29	2.41	123
Nazc-Pacf	−88.866	55.680	1.283 ± 0.013	1.02	0.29	80
Nazc-Soam	87.680	52.913	0.623 ± 0.013	2.06	0.59	83
Pacf-Soch	94.142	−64.847	0.981 ± 0.011	0.41	0.19	169
Sina-Arab	64.424	21.074	0.031 ± 0.145	159.34	4.9	152
Sina-Nubi	31.555	31.506	0.526 ± 0.132	1.54	0.31	11
Soch-Eura	−0.395	55.495	0.084 ± 0.010	22.98	2.33	5

[a]Plate abbreviations are given in Table 1. The first plate rotates CCW relative to the second plate. All uncertainties are unscaled.

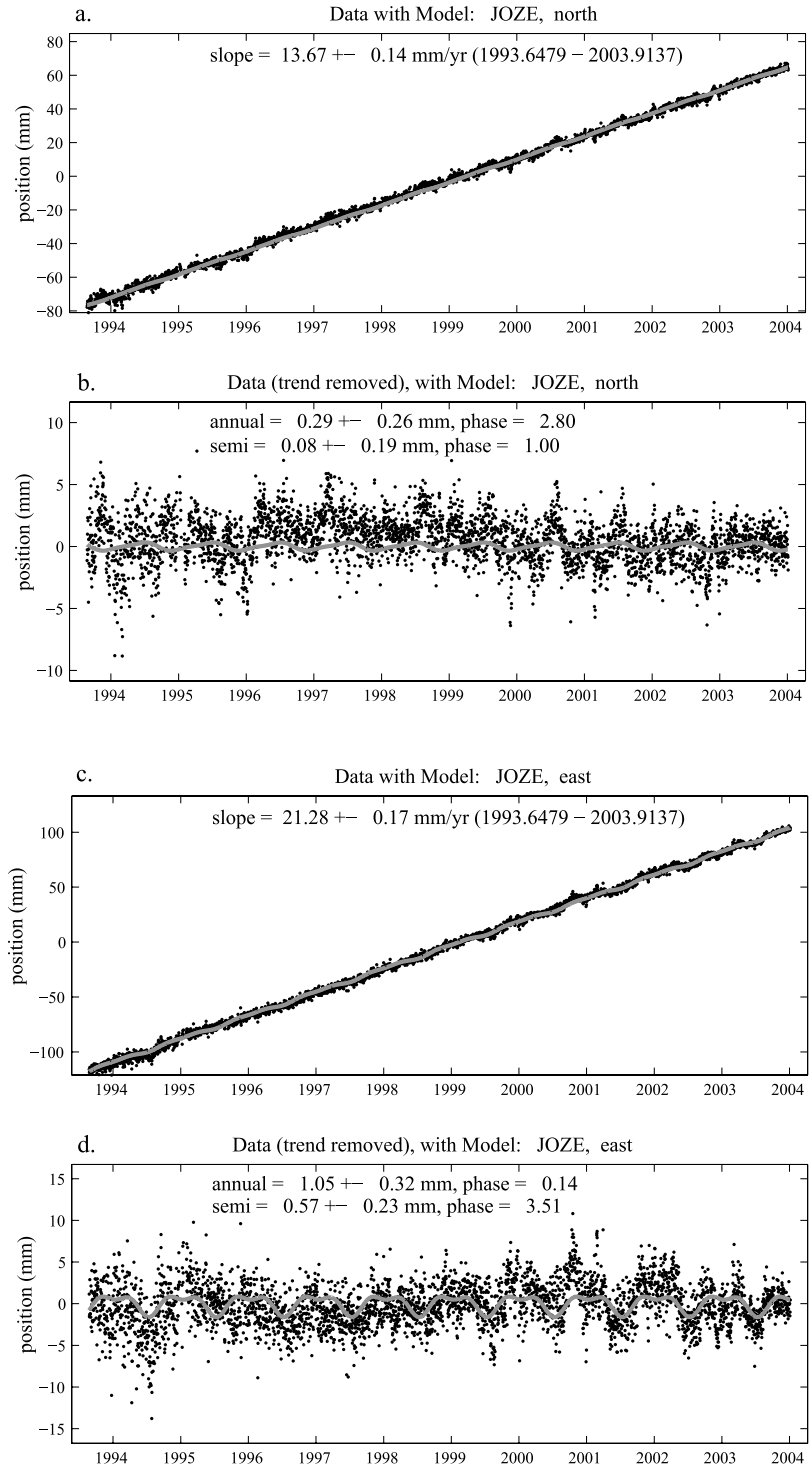

Figure 3. Example time series showing the (a and b) north and (c and d) east position time series for station JOZE (Jozefoslaw, Poland) with modeled (gray lines) trends and annual and semiannual fluctuations. Figures 3b and 3d show data with the trend removed.

sites affected by improperly modeled coseismic and postseismic deformation. Combining results from diverse analysis centers assumes that the whole is greater than the sum of its parts. This is only true if the noise characteristics of these solutions are white, which we know not to be the case at least for continuous GPS data [*Zhang et al.*, 1997], and devoid of systematic errors. It is therefore beneficial, for comparison purposes, to perform a study using only one type of data (CGPS) analyzed in wholly consistent manner.

[17] Our plate angular velocities in ITRF2000 (listed in Table 2) are generally consistent with *Sella et al.*'s [2002], which are estimated in ITRF97. To compare our plate angular velocities, we converted the values in Table 2 into Cartesian coordinates and differenced them with the

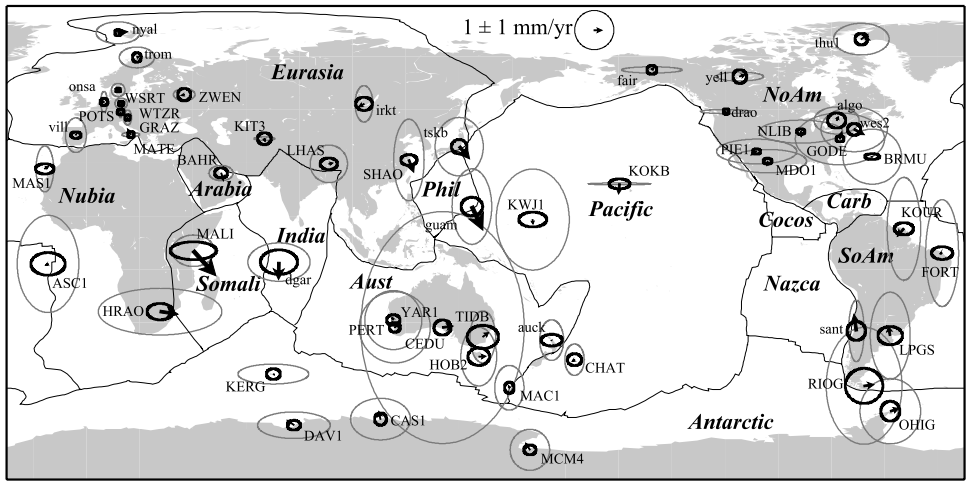

Figure 4. Differences between our velocity estimates for the IGS core stations and the official ITRF2000 velocities, with comparison of velocity error ellipses (95% confidence) of IGS core sites derived from this study with ITRF2000 official velocity error ellipses. Our estimates use a white noise plus flicker noise model for the underlying position time series. Ellipses derived from this study are drawn in thicker line.

corresponding values in *Sella et al.*'s [2002] study. The largest difference, on the order of 1°/Myr occurs for the Sierra plate, which is not surprising since it is a relatively small block located in an intensely deforming boundary zone. Excluding the Sierra and Sinai plates (*Sella et al.* [2002] do not estimate an angular velocity for the Sinai plate), the RMS differences between *Sella et al.*'s [2002] ITRF97 angular velocities and our ITRF2000 angular velocities are on the order of 0.01°/Myr for all three (*X*, *Y*, *Z*) components. In most cases, our pole error ellipses are smaller than those estimated by previous studies, reflecting our lower velocity uncertainties.

[18] We also estimate vertical velocities in ITRF2000 for all stations (Table 1 and Figure 5). The vertical rate uncertainty ranges from 0.5 to 1.2 mm/yr for stations with time series of 5 years or longer. The vertical rate is significant for several stations in northwestern Europe, North America, and Antarctica, where the effects of glacial isostatic adjustment (GIA) are expected.

[19] In North America, vertical rates at algo, chur, dubo, flin, nrc1, sch2, and yell suggest that the uplift rates are highest around Hudson Bay and decrease radially outward, which is generally consistent with the spatial pattern of predicted vertical rates due to GIA [e.g., *Peltier*, 1998].

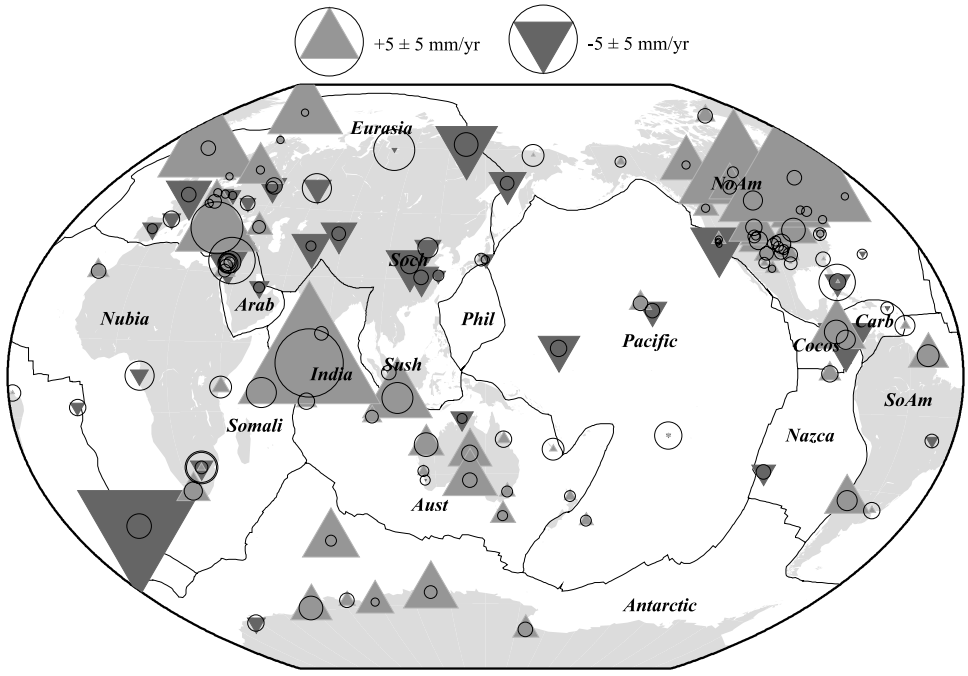

Figure 5. Vertical station velocities in ITRF2000. Light gray triangles indicate uplift, and inverted dark gray triangles indicate subsidence. Circles are 1σ uncertainties.

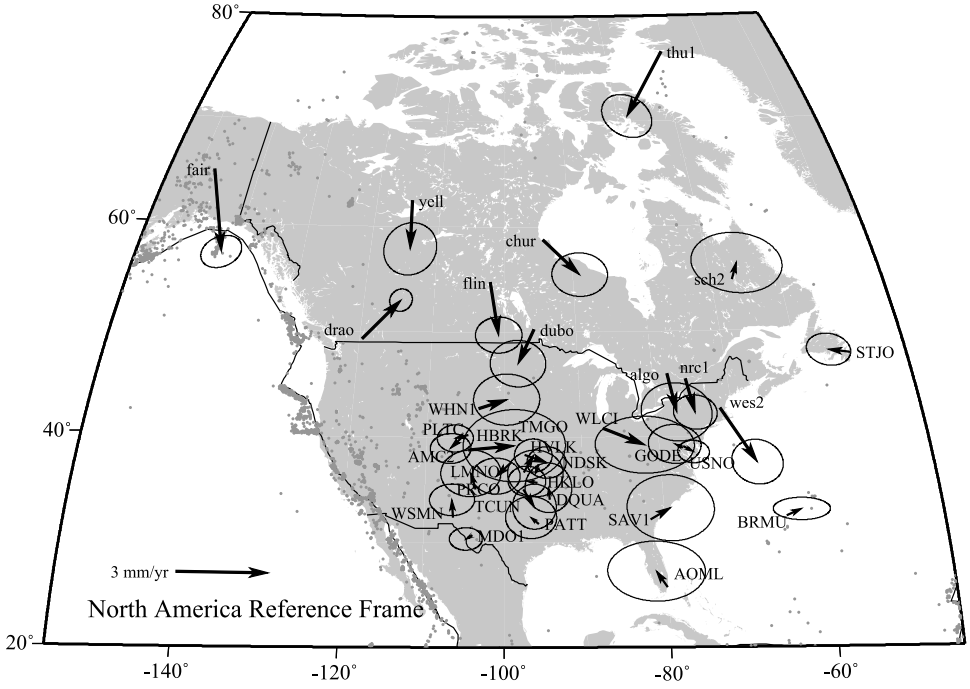

Figure 6. Residual velocities relative to North America. Stations used to define North American plate rotation are labeled in capital letters. Ellipses indicate 2-D 95% confidence limits.

We compared our vertical rates at stations algo, chur, fair, drao, wes2, and yell with values for those sites predicted by *Peltier* [1995] based on the ICE-4G deglaciation model. Our vertical rate estimates for these stations are all larger than the predicted rates, with a mean difference of 1.1 mm/yr.

[20] In northwestern Europe the vertical rate is significant at stations nyal, mets, and hofn and considerably smaller at onsa and trom. The vertical deformation at nyal, onsa, and trom is largely consistent with the pattern predicted by *Lambeck et al.* [1998]. The differences between our vertical rate estimates and vertical rates predicted by *Peltier* [1995] are 0.9 mm/yr for station mets, 6.5 mm/yr for nyal, −0.4 mm/yr for onsa, and −0.1 mm/yr for trom.

[21] Euler vectors are well determined for the North American, Eurasian, Australian, and Pacific plates. The χ^2_ν values are close to unity (without the need for a posteriori scaling), suggesting good fit to rigid plate rotation and realistic uncertainty estimates. Residual velocities for these four plates are generally well below 1 mm/yr. Large χ^2_ν values for the Nazca and Sunda Shelf plates indicate that the plate parameters are not well determined from the limited set of station velocities. A χ^2_ν value of much less than one for our South America Euler vector may indicate that the station velocity uncertainties are overestimated. Stations in South America have long shown large seasonal fluctuations and higher-than-average noise levels which result in larger velocity uncertainties. Below we discuss a few noteworthy aspects of some of the tectonic plates/blocks for which we estimate Euler vectors.

3.1. North American Plate

[22] Our Euler vector for the North American plate is one of the best determined estimates (mean rate residual of 0.6 mm/yr, $\chi^2_\nu = 1.3$), including velocities from 22 stations with uncertainties ranging from 0.1 to 0.6 mm/yr. It is in good agreement with estimates by *Beavan et al.* [2002] and *Sella et al.* [2002]. We excluded stations algo, chur, drao, fair, wes2, and yell, which are expected to be experiencing vertical deformation due to GIA. The large residual velocities at these stations (Figure 6) suggest that the horizontal rates are also affected by GIA.

3.2. Eurasian Plate

[23] Our Euler vector for the Eurasian plate, estimated using velocities at 18 stations which extend from heavily instrumented western Europe to Tixi in the NE Russian Federation, is well determined (0.002°/Myr in pole angular velocity, 0.8° in semimajor axis, $\chi^2_\nu = 1.1$). Residual velocities relative to our estimated Eurasia reference frame are shown in Figure 7. We excluded stations nyal, onsa, and trom in Scandinavia from the Eurasian plate estimation because we expect them to be affected by GIA [*Peltier*, 1998]. Station irkt, a core IGS station located on the western flank of the Baikal rift, was also excluded from the plate rotation estimation because of large residual velocities which suggest that it is located in a zone of deformation. Paleoseismic data suggest recent (Holocene) seismic activity along the lower Rhine graben [*Meghraoui et al.*, 2000]. We excluded stations brus and kosg, which are located within 100 km of the Rhine graben because they show large residual velocities (>3 mm/yr). Three stations located west of the Rhine Graben (hers, toul, and vill) show good fit to the Eurasian plate (Table 1). Nevertheless, we follow the conservative approach of *Sella et al.* [2002] and exclude these stations from our formal Eurasian plate definition. Currently, Eurasia appears as a rigid plate extending from western Europe (west of the Rhine graben) to NE Russia. However, velocity error ellipses in eastern Europe and central Asia are significantly larger than those in western Europe (Figure 7).

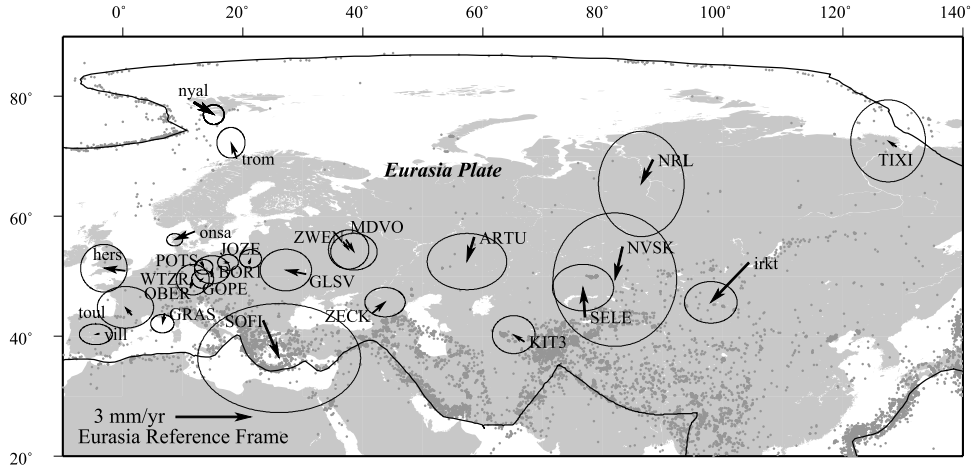

Figure 7. Residual velocities relative to Eurasia. Stations used to define Eurasian plate rotation are labeled in capital letters. Ellipses indicate 2-D 95% confidence limits.

As these error ellipses shrink with time, we will be able to reevaluate the extent of the rigid Eurasian plate.

3.3. Antarctic Plate

[24] In estimating Euler vectors for North America and Eurasia we have excluded stations which are affected by GIA. We expect that most, if not all, of the stations in Antarctica are affected by GIA, as evidenced by their large vertical rates (Table 1). Therefore, in estimating the Euler vector for Antarctica we do not exclude any stations on the basis of expected GIA. Station maw1 was excluded because of its large residual velocity. In spite of the presumable effect of GIA, the Euler vector for Antarctica is relatively well determined (mean rate residual of 0.8 mm/yr, $\chi^2_\nu = 1.6$).

3.4. Pacific Plate

[25] Our estimate for Pacific plate rotation uses velocities from five sites but is well determined (mean rate residual of 0.8 mm/yr, $\chi^2_\nu = 1.2$) and in good agreement with *Beavan et al.*'s [2002] estimate which includes data from 11 stations. Station farb on the Farallon islands shows 2.7 mm/yr of residual motion relative to the Pacific plate, suggesting that it is affected by the plate boundary zone in northern California. We currently process data from the SCIGN station guax on Guadalupe Island, but the time series by July 2003 was only 1 year long and had experienced a period of data communications problems, so we do not include the velocity at guax in our Pacific plate estimation. On the basis of our study of survey stations on Guadalupe [*Gonzalez-Garcia et al.*, 2003] and our recent SOPAC time series (circa July 2004), the velocity of station guax now provides an important additional constraint for Pacific plate motion and is used in our monthly plate motion model updates.

3.5. Australian Plate

[26] We estimate Australian plate motion using velocities at nine stations in Australia, including Tasmania. Site velocity uncertainties for these sites on the Australian plate are ~0.5 mm/yr, somewhat less precise than sites in the Northern Hemisphere. Nevertheless, misfits to the plate motion model are all within 1 mm/yr, and the Euler vector is well determined (0.003°/Myr, 0.9° in semimajor axis, $\chi^2_\nu = 1.2$). We exclude three stations in the region from full Australian plate motion with misfits of ~2 mm/yr. Auckland (auck) and Noumea (noum), both IGS core stations, have large (>2 mm/yr) misfits to rigid Australian plate motion, suggesting that they are affected by (Australian-Pacific) plate boundary deformation. We also exclude Cocos Island (coco), also an IGS core station, in the transition zone between the Australian and Indian plates.

3.6. Sierra Plate

[27] We estimate an Euler vector for the Sierra block that is significantly different from *Sella et al.*'s [2002]. We use only three stations in the Sierra plate estimation (*Sella et al.* [2002] used nine stations) (Tables 1 and 2). Our estimated rotation rate for the Sierra plate is up to twice as fast, but our rotation rate uncertainty is high (Table 2), and within this uncertainty the rotation rate is still consistent with *Sella et al.*'s [2002] estimate.

3.7. Indian Plate

[28] Two stations in India (hyde and IISC) and one in the Maldives (MALD) are moving more than 10 mm/yr relative to Australia. The time series at hyde is <1 year long, so we use only velocities from IISC and MALD to estimate a rotation vector for the Indian plate. Station hyde is most likely located on the rigid part of the Indian plate [*Sella et al.*, 2002], but its velocity uncertainties are still much too large to provide additional constraint.

3.8. South China and Sunda Shelf Plates

[29] We estimate an Euler vector for the South China plate using three stations, SHAO, WUHN, and XIAN. Since the distribution of publicly available CGPS stations in this region is rather sparse, we included XIAN even though it is located north of the Qinling fault (Figure 8). In another GPS study, *Shen et al.* [2000] noted that there is no apparent motion between XIAN and WUHN. The three stations fit the South China plate well (Table 1), consistent with *Shen et al.*'s [2000] study. Stations NTUS in Singapore and BAKO in Java show significant motion relative to South China (Figure 8). We estimate an Euler vector for the Sunda Shelf plate using these two stations. The Euler vector for the Sunda Shelf is not well constrained (Table 2) from the current distribution of CGPS stations. A recent paper based

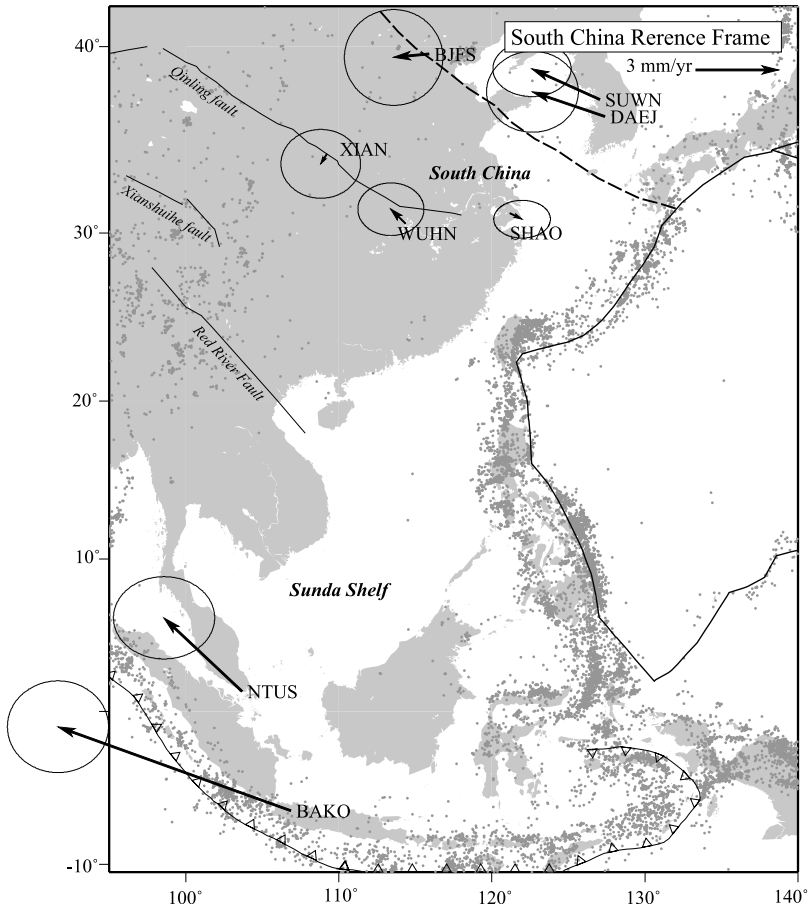

Figure 8. Residual velocities relative to South China. Stations used to define South China plate rotation are labeled in capital letters. Ellipses indicate 2-D 95% confidence limits.

primarily on survey mode GPS provides better constraints on Sunda Shelf motion [*Bock et al.*, 2003].

3.9. Amurian and Okhotsk Plates

[30] Discussion of the plate boundary region between Eurasia and North America, located in east Asia, has included smaller plates to explain the regional tectonics. *Zonenshain and Savostin* [1981] proposed an Amurian plate, covering northeast China, Korea, the Japan Sea, and SE Russia, which moves eastward up to 10 mm/yr relative to the Eurasian plate. *Seno et al.* [1996] proposed the existence of an Okhotsk plate along the eastern margin of the Japan Sea. *Sella et al.* [2002] estimate a rotation pole for the Amurian plate using GPS stations in South Korea and in Vladivostok. In contrast, a study of GPS observations by *Steblov et al.* [2003] shows that an Amurian plate is not required. Our velocities for three stations located on the postulated Amurian plate (DAEJ and SUWN in South Korea and BJFS in Beijing, China) show significant motion (>3 mm/yr) relative to Eurasia (Figure 9). We estimate an Euler vector for the Amurian plate using velocities at these three stations. Our estimated Euler vector for the Amurian plate is not well constrained and is statistically indistinguishable from that of the South China plate (Table 2). Relative to the South China plate, BJFS, DAEJ, and SUWN have residual velocities of up to 2.7 mm/yr. While the velocities of these stations are significantly different from both Eurasia and South China motions, they do not fit a single Euler vector well and may therefore represent a region of diffuse deformation between Eurasia and South China instead of a separate microplate. Although we have data from four stations (petp, tskb, usud, and yssk) which are potentially located on the Okhotsk plate, the velocities at these sites do not fit a single Euler vector well. These stations are located close to the Japan and Kuril trenches and may be affected by subduction at these trenches.

3.10. Arabian and Sinai Plates

[31] Data from the eastern Mediterranean array are archived and processed at SOPAC and are included in this study. Modeling of these data by *Wdowinski et al.* [2004] has shown a slip rate of 3.3 ± 0.5 mm/yr along the Dead Sea fault, clearly showing separation of the Sinai block from the Arabian plate. We therefore estimate rotation parameters for a Sinai block separate from the Arabian plate. The Arabian and Sinai plate Euler poles are located very close to each other (Table 2), and the relative Arabian-Sinai rotation pole is not well defined (Table 3).

[32] There are currently no continuous GPS stations on the Cocos plate (the Cocos plate lies entirely under water, so its motion cannot be measured using GPS) and only one publicly available continuous station each on the Anatolian and Philippine Sea plates. Therefore we are presently unable to estimate Euler vectors for these three plates. (*Sella et al.*

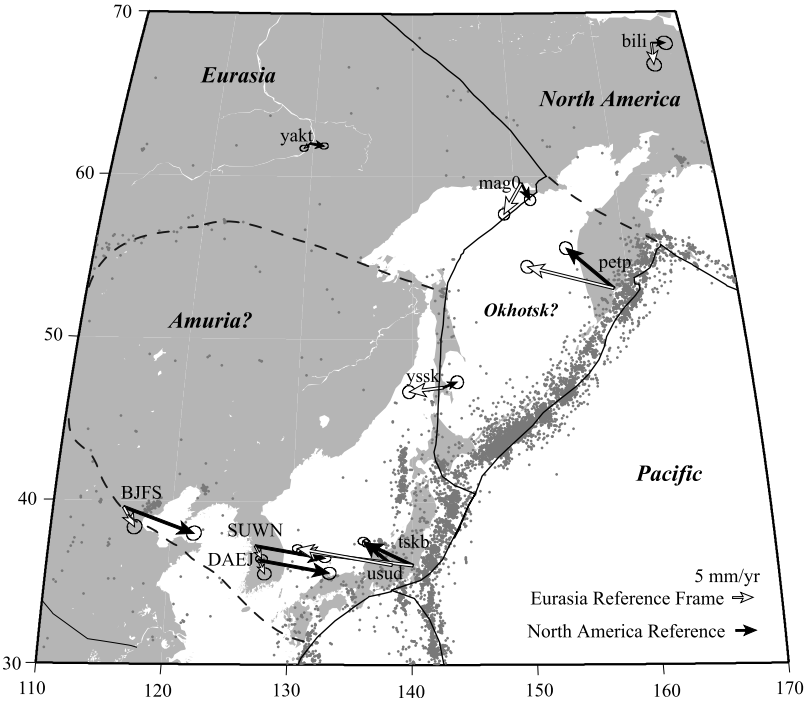

Figure 9. Residual velocities in eastern Asia relative to Eurasia (clear arrows) and North America (solid arrows). Ellipses indicate 2-D 95% confidence limits.

[2002] estimated angular velocities for the Philippine and Anatolian plates with the help of survey GPS and SLR data.)

[33] Several stations which are ITRF2000 reference stations (noted in Table 1) are shown by this study to be located not on rigid plate and may be affected by regional tectonics. Since our rigid plate rotation estimates are consistent (although more precise) with other studies, it appears that inclusion of these sites in the definition of ITRF2000 does not result in any detectable bias. This is probably because the IGS constraints for many of these stations are looser than those suggested by our study (Figure 4).

4. Summary

[34] We present Euler vectors for 17 major and minor tectonic plates on the basis of a rigorous analysis of CGPS stations and their position time series. Our results are generally consistent with previous studies [e.g., *Beavan et al.*, 2002; *Sella et al.*, 2002] but are more precise. For the North American, Eurasian, Australian, and Antarctic plates our data constrain the rotation pole locations to <1° and the rotation rates to <0.006°/Myr. Although only five stations are available for the Pacific plate, the Euler vector estimate for the Pacific plate is as good (Table 2). More permanent CGPS stations with publicly available data are needed in order to resolve angular velocities for the Philippine, Okhotsk, Amurian, Anatolian, and Somali plates.

[35] Vertical rates in northwestern Europe, Canada, and Antarctica suggest glacial isostatic adjustment that are, in general, consistent with recent studies and predictions and appear to be promising for more detailed studies and testing against various models.

[36] The IGS realization of ITRF2000 is currently (at the time of this writing) going through revision (to IGS2000 version 2), with the number of core sites being expanded to include 99 CGPS stations. Many of the stations newly designated as core sites in IGS2000 version 2 are used here for rigid plate definitions. However, our analysis also reveals that several of these reference stations may be located in deforming plate boundary zones (Table 1). Continued use of these stations as reference/fiducial sites requires caution as they have the potential to exhibit non-secular motion due to slip along the plate boundaries.

[37] The main results of this paper are the Euler vectors presented in Table 2. However, for the more poorly determined plates we expect the Euler vectors to improve with time as the velocity uncertainties grow smaller. As the number of global stations increase and the existing time series grow over the years, some of the plate rotation parameters may have to be revised, particularly those in eastern Asia, where the question of the Amurian and Okhotsk microplates remains unresolved.

[38] **Acknowledgments.** We thank the IGS (http://igscb.jpl.nasa.gov/) for facilitating the availability of global GPS data and our fellow IGS Global Data Centers, NASA's CDDIS (http://cddisa.gsfc.nasa.gov/cddis_welcome.html) and the IGN (http://igs.ensg.ign.fr/). The use of regional GPS data from various sources is acknowledged; a complete list of regional arrays can be found at http://sopac.ucsd.edu/maps/. We thank Peng Fang and Paul Jamason at SOPAC for providing precise orbits and GPS solutions (global and regional). Constructive comments by Associate Editor Freysteinn Sigmundsson, John Beavan, and an anonymous reviewer greatly improved our paper. This study was funded by the Southern California Earthquake Center through its support for the analysis of Southern California Integrated GPS Network (SCIGN) data.

References

Altamimi, Z., P. Sillard, and C. Boucher (2002), ITRF2000: A new release of the International Terrestrial Reference Frame for earth science applications, *J. Geophys. Res.*, *107*(B10), 2214, doi:10.1029/2001JB000561.

Altamimi, Z., P. Sillard, and C. Boucher (2003), The impact of a no-net rotation condition on the ITRF2000, *Geophys. Res. Lett.*, *30*(2), 1064, doi:10.1029/2002GL016279.

Argus, D., and R. G. Gordon (1991), No-net-rotation model of current plate velocities incorporating plate motion models NUVEL-1, *Geophys. Res. Lett.*, *18*, 2039–2042.

Beavan, J., P. Tregoning, M. Bevis, T. Kato, and C. Meertens (2002), Motion and rigidity of the Pacific plate and implications for plate boundary deformation, *J. Geophys. Res.*, *107*(B10), 2261, doi:10.1029/2001JB000282.

Blewitt, G., and D. Lavallee (2002), Effect of annual signals on geodetic velocity, *J. Geophys. Res.*, *107*(B7), 2145, doi:10.1029/2001JB000570.

Blewitt, G., et al. (1993), Absolute far-field displacements from the June 28, 1992, Landers earthquake sequence, *Nature*, *361*, 340–342.

Bock, Y., et al. (1993), Detection of crustal deformation from the Landers earthquake sequence using continuous geodetic measurements, *Nature*, *361*, 337–340.

Bock, Y., L. Prawirodirdjo, J. F. Genrich, C. W. Stevens, R. McCaffrey, C. Subarya, S. S. O. Puntodewo, and E. Calais (2003), Crustal motion in Indonesia from GPS measurements, *J. Geophys. Res.*, *108*(B8), 2367, doi:10.1029/2001JB000324.

Bock, Y., L. Prawirodirdjo, and T. I. Melbourne (2004), Detection of arbitrarily large dynamic ground motions with a dense high-rate GPS network, *Geophys. Res. Lett.*, *31*, L06604, doi:10.1029/2003GL019150.

Chase, C. G. (1972), The n-plate problem of plate tectonics, *Geophys. J. R. Astron. Soc.*, *29*, 117–122.

Chase, C. G. (1978), Plate kinematics: The Americas, East Africa, and the rest of the world, *Earth Planet. Sci. Lett.*, *37*, 355–368.

Christodoulidis, D. C., D. E. Smith, R. Kolenkiewicz, S. M. Klosko, M. H. Torrence, and P. J. Dunn (1985), Observing tectonic plate motions and deformations from satellite laser ranging, *J. Geophys. Res.*, *90*, 9249–9263.

DeMets, C., and T. H. Dixon (1999), New kinematic models for Pacific-North America motion from 3 Ma to present. I. Evidence for steady motion and biases in the NUVEL-1A model, *Geophys. Res. Lett.*, *26*, 1921–1924.

DeMets, C., R. Gordon, D. Argus, and S. Stein (1994), Effects of recent revisions to the geomagnetic reversal time scale on estimates of current plate motions, *Geophys. Res. Lett.*, *21*, 2191–2194.

Dixon, T., A. Mao, and S. Stein (1996), How rigid is the stable interior of the North American plate?, *Geophys. Res. Lett.*, *23*, 3035–3038.

Dragert, H., K. Wang, and T. James (2001), A silent slip event on the deeper Cascadia subduction interface, *Science*, *292*, 1525–1528.

Drewes, H. (1998), Combination of VLBI, SLR, and GPS determined station velocities for actual plate kinematic and crustal deformation models, in *Geodesy on the Move: Gravity, Geoid, Geodynamics and Antarctica: IAG Scientific Assembly, Rio de Janeiro, Brazil, September 3–9, 1997*, *IAG Symp.*, vol. 119, edited by R. Forsberg, M. Feissel, and R. Dietrich, pp. 377–382, Springer-Verlag, New York.

Gonzalez-Garcia, J. J., L. Prawirodirdjo, Y. Bock, and D. Agnew (2003), Guadalupe Island, Mexico, as a new constraint for Pacific plate motion, *Geophys. Res. Lett.*, *30*(16), 1872, doi:10.1029/2003GL017732.

Herring, T. (2000), Global Kalman filter VLBI and GPS analysis program (GLOBK), version 5.0, Mass. Inst. of Technol., Cambridge.

Herring, T. A., et al. (1986), Geodesy by radio interferometry: Evidence for contemporary plate motion, *J. Geophys. Res.*, *91*, 8341–8347.

King, R., and Y. Bock (2002), Documentation for the GAMIT GPS analysis software, release 10.06, Mass. Inst. of Technol., Cambridge.

Kreemer, C., and W. E. Holt (2001), A no-net-rotation model of present-day surface motions, *Geophys. Res. Lett.*, *28*, 4407–4410.

Kreemer, C., W. E. Holt, and A. J. Haines (2003), An integrated global model of present-day plate motions and plate boundary deformation, *Geophys. J. Int.*, *154*, 8–34.

Lambeck, K., C. Smither, and M. Ekman (1998), Tests of glacial rebound models for Fennoscandinavia based on instrumented sea-and lake-level records, *Geophys. J. Int.*, *135*, 375–387.

Larson, K., J. Freymueller, and Philipsen (1997), Global plate velocities from the Global Positioning System, *J. Geophys. Res.*, *102*, 9961–9982.

Larson, K., P. Bodin, and J. Gomberg (2003), Using 1-Hz GPS data to measure deformations caused by the Denali Fault earthquake, *Science*, *300*, 1421–1424.

Le Pichon, X., J. Francheteau, and J. Bonnin (1973), *Plate Tectonics*, 302 pp., Elsevier Sci., New York.

McKenzie, D. P., and R. L. Parker (1967), The North Pacific: An example of tectonics on a sphere, *Nature*, *216*, 1276–1280.

Meghraoui, M., T. Camelbeeck, K. Vanneste, M. Brondeel, and D. Jongmans (2000), Active faulting and paleoseismology along the Bree fault, lower Rhine graben, Belgium, *J. Geophys. Res.*, *105*, 13,809–13,842.

Melbourne, T. I., and F. H. Webb (2002), Precursory transient slip during the 2001 M_w = 8. 4 Peru earthquake sequence from continuous GPS, *Geophys. Res. Lett.*, *29*(21), 2032, doi:10.1029/2002GL015533.

Melbourne, T. I., F. H. Webb, J. M. Stock, and C. Reigber (2002), Rapid postseismic transients in subduction zones from continuous GPS, *J. Geophys. Res.*, *107*(B10), 2241, doi:10.1029/2001JB000555.

Miller, M. M., T. Melbourne, D. J. Johnson, and W. Q. Sumner (2002), Periodic slow earthquakes from the Cascadia Subduction Zone, *Science*, *295*, 2423.

Minster, J. B., and T. H. Jordan (1978), Present-day plate motions, *J. Geophys. Res.*, *83*, 5331–5534.

Minster, J. B., T. H. Jordan, P. Molnar, and E. Haines (1974), Numerical modeling of instantaneous plate tectonics, *Geophys. J. R. Astron. Soc.*, *36*, 541–576.

Miyazaki, S., Y. Hatanaka, T. Sagiya, and T. Tada (1998), The nationwide GPS array as an Earth observation system, *Tech. Rep. Bull. Geogr. Surv. Inst.*, *44*, 11–22.

Morgan, W. J. (1968), Rises, trenches, great faults, and crustal blocks, *J. Geophys. Res.*, *73*, 1959–1982.

Morgan, W. J. (1971), Convection plumes in the lower mantle, *Nature*, *230*, 42–43.

Morgan, W. J. (1972), Deep mantle convection plumes and plate motions, *Bull. Am. Assoc. Pet. Geol.*, *56*, 203–213.

Nikolaidis, R. (2002), Observation of geodetic and seismic deformation with the Global Positioning System, Ph.D. thesis, Univ. of Calif., San Diego.

Nikolaidis, R. M., Y. Bock, P. J. de Jonge, P. Shearer, D. C. Agnew, and M. Van Domselaar (2001), Seismic wave observations with the Global Positioning System, *J. Geophys. Res.*, *106*, 21,897–21,916.

Norabuena, E. O., T. H. Dixon, S. Stein, and C. G. A. Harrison (1999), Decelerating Nazca-South America and Nazca-Pacific plate motions, *Geophys. Res. Lett.*, *26*, 3405–3408.

Peltier, W. R. (1995), VLBI baseline variations from the ICE-4G model of postglacial rebound, *Geophys. Res. Lett.*, *22*, 465–468.

Peltier, W. R. (1998), A space geodetic target for mantle viscosity discrimination: Horizontal motions induced by glacial isostatic adjustment, *Geophys. Res. Lett.*, *25*, 543–546.

Sella, G. F., T. H. Dixon, and A. L. Mao (2002), REVEL: A model for recent plate velocities from space geodesy, *J. Geophys. Res.*, *107*(B4), 2081, doi:10.1029/2000JB000033.

Seno, T., T. Sakurai, and S. Stein (1996), Can the Okhotsk plate be discriminated from the North American plate?, *J. Geophys. Res.*, *101*, 11,305–11,315.

Shen, Z. K., D. D. Jackson, Y. Feng, M. Cline, M. Kim, P. Fang, and Y. Bock (1994), Postseismic deformation following the Landers earthquake, California, 28 June 1992, *Bull. Seismol. Soc. Am.*, *84*, 780–791.

Shen, Z., C. Zhao, A. Yi, Y. Li, D. D. Jackson, P. Fang, and D. Dong (2000), Contemporary crustal deformation in east Asia constrained by Global Positioning System measurements, *J. Geophys. Res.*, *105*, 5721–5734.

Solomon, S. C., and N. H. Sleep (1974), Some simple physical models for absolute plate motions, *J. Geophys. Res.*, *79*, 2557–2567.

Steblov, G. M., M. G. Kogan, R. W. King, C. H. Scholz, R. Burgmann, and D. I. Frolov (2003), Imprint of the North American plate in Siberia revealed by GPS, *Geophys. Res. Lett.*, *30*(18), 1924, doi:10.1029/2003GL017805.

Wdowinski, S., Y. Sudman, and Y. Bock (2001), Geodetic detection of active faults in S. California, *Geophys. Res. Lett.*, *28*, 2321–2324.

Wdowinski, S., Y. Bock, G. Baer, L. Prawirodirdjo, N. Bechor, S. Naaman, R. Knafo, Y. Forrai, and Y. Melzer (2004), GPS measurements of current crustal movements along the Dead Sea Fault, *J. Geophys. Res.*, *109*, B05402, doi:10.1029/2003JB002793.

Williams, S. D. P. (2003), The effect of coloured noise on the uncertainties of rates estimated from geodetic time series, *J. Geod.*, *76*, 483–494.

Williams, S. D. P., Y. Bock, P. Fang, P. Jamason, R. M. Nikolaidis, L. Prawirodirdjo, M. Miller, and D. J. Johnson (2004), Error analysis of continuous GPS position time series, *J. Geophys. Res.*, *109*, B03412, doi:10.1029/2003JB002741.

Wilson, J. T. (1963), A possible origin of the Hawaiian Islands, *Can. J. Phys.*, *41*, 863–870.

Wilson, J. T. (1965), Evidence from ocean island suggesting movement in the Earth, *Philos. Trans. R. Soc. London*, *258*, 145–165.

Zhang, J. (1996), Continuous GPS measurements of crustal deformation in southern California, Ph.D. thesis, Univ. of Calif., San Diego.

Zhang, J., Y. Bock, H. Johnson, P. Fang, S. Williams, J. Genrich, S. Wdowinski, and J. Behr (1997), Southern California Permanent GPS Geodetic Array: Error analysis of daily position estimates and site velocities, *J. Geophys. Res.*, *102*, 18,035–18,055.

Zonenshain, L. P., and L. A. Savostin (1981), Geodynamics of the Baikal rift zone and plate tectonics of Asia, *Tectonophysics*, *76*, 1–45.

Y. Bock and L. Prawirodirdjo, Institute of Geophysics and Planetary Physics, Scripps Institution of Oceanography, University of California, San Diego, 9500 Gilman Dr., La Jolla, CA 92093-0225, USA. (ybock@ucsd.edu; linette@josh.ucsd.edu)